Cascades of Secondary Particles in High Voltage Accelerators

M. Cavenago*[1], P. Antonini[1,3], P. Veltri[2], N. Pilan[2], V. Antoni[2], G. Serianni[2]
[1]INFN/LNL, Lab. Nazionali di Legnaro, [2]RFX, Assoc. Euratom-ENEA, [3]Centro Ric. E. Fermi, Roma
*corresponding author: viale dell'Universita' n. 2, I-35020, Legnaro (PD), Italy; cavenago@lnl.infn.it

Abstract: A simplified system for high voltage test is studied, with the am of understanding the reasons for failures of voltage holding which are not covered by conventional and local design criteria. A first understanding of the problem is obtained by solving the electrostatic potential in a 2D axisymmetric geometry with Comsol Multiphysics; the detail of the electrode shapes is taken into account and a cascade of particles between opposite electrodes is generated: the impact of an ion (say a H^+) with an electrode extracts particles of the opposite charge (say electrons, H^-) which are in turn accelerated in the opposite direction. Electrons are treated relativistically. Very specific attractors were found for the impact points; physical reason is that the highly non uniform electric field may focus, defocus or move the discharge. A second analysis takes into account the spread of the reemitted particle velocity and a consequent 3D motion. Solution of a Fokker Planck style equation for the impact point confirms the existence of hot spots. Plans to include perturbations to azimuthal geometry are noted.

Keywords: microdischarge, negative ion, high voltage, statistical average

1 Introduction

In a high voltage accelerator system, we study the effect of a cascade of particle emission between opposite electrodes (named also pingpong for obvious analogy), which is probable in some surface conditions; with a simple postprocessor application, we show that the cascade moves spatially and tends to converge at some particular electrode positions, which are named attractors. In 2D, the attractor position does match the observed damage on some real electrodes (seemingly not the weakest point on the electrode). So that a prediction of failures and remedies seems here possible and motivate further study and prelimary work on extension to 3D model and on statistical models, here also presented.

The holding of high voltages > 100 kV (HV) has a reputation for being a subject of difficult predictability and repeatability. Phenomena of microdischarges between the electrodes of high voltage accelerating tubes are common, but their physical aspects are not yet fully understood [1, 2, 3]. Part of the subject complexity is due to the fact that the large variety of accelerator applications leads to different electrode conditions, and the accelerator itself is made from several parts, so that different systems are actually covered; another reason is due to uncertainities of surface preparation. Other phenomena are more clearly related to multiphysics modelling, as the fact that a current leakage may heat an electrode (which is a positive feedback, leading to a spark) or may clean the electrode, which reduces emission and is a negative feedback, leading to a short transient discharge (named spike).

Even if HV systems are designed not to exceed by a good safety margin a given surface field over which field emission is possible, there are at least three known mechanisms for the onset of discharge in vacuum, discussed in the literature[2] and relevant here: 1) isolator surface discharge; for example when an electron strikes an insulator, it may produce on average δ secondary electrons; when $\delta > 1$, the insulator surface charges up and design fields are altered locally, with possible discharge (also in relation to adsorbed gas or imperfection in the isolator or in its junction to the electrode); remedy mainly consists in modifying the design, to obtain a lower field near the junction; 2) microparticle emission; let V_1 be the anode to catode voltage and d their distance; if a microparticle detaches from the anode,

it will get a positive charge ($\propto V_1/d$) by induction and will impinge on the catode with an energy ($\propto V_1^2/d$), which may be sufficient to locally melt the electrode and to trigger a discharge; otherwise the microparticle may bounce, getting a negative charge by induction (and repeat the process); by postulating microparticle emission, Cranberg[3] was able to predict a $V_1 \propto \sqrt{d}$ trend; 3) microdischarge by regenerative ion emission, which will be here studied in detail; an H^+ ion emitted from the anode impinges on the catode, extracting negative particles, including an average number μ_- of H^- from hydrogen or pump oil absorbed on the catode); in turn each H^- accelerated against the anode extracts an average number μ_+ of H^+ ions. According to Ref. [1], when $\mu = \mu_-\mu_+ > 1$ current rises until absorbed contaminants decrease, so that μ become less than 1 and discharge decreases; further studies assuming parallel electrodes and an emitted particle velocity distribution[4] conclude that the discharge spreads over these electrodes and thus weakens.

Fig. 1 show a test geometry for high voltage devices (about 1 MV) in the style of a Cockroft-Walton accelerator. One electrode protrudes towards the other, so to obtain a higher acceleration field. This design incorporates and exemplifies several good design practices: 1) the point of maximum electric stress is rounded; 2) the necessary support of the catode is made from several insulators, separated by large metal electrodes, so that the voltage step per insulator is reduced (200 kV) and insulators are protected from particle and X-ray impact; 3) the distances between the anode and these intermediate electrodes increase with the voltage difference between them.

A similar geometry was also used in some voltage tests of ion sources, considered for Neutral Beam Injectors (NBI) in fusion devices, in the 800 kV to 1 MV range [5, 6, 8], with even better insulator design and protection; anode also contain a drift tube (not shown in fig 1) to transport the beam produced from the ion source (also not shown in fig 1). In some experimental conditions, a fairly large pressure of H_2 gas [10^{-3} Pa or more] was required; holding the 800 kV voltage proved difficult, and after experiment some burning was apparent on the anode, at about four azimuthal positions[6], approximately at the same r, z marked in fig 1.

In section II, after introducing the electrostatic model and the ray tracing equation, simulation results from Comsol Multiphysics (CM) will prove in a straighforward manner that a microdischarge does compress near the attractor, giving the so-called hot spots on the electrodes. In the voltage range considered, electrons are strongly subjected to relativistic effects, so the implemented equations are fully relativistic. In section III, we briefly recall a full 3D statistical theory, which very approximately gives a Fokker Planck equation for the anode emitted current, where μ is an eigenvalue and coefficients have to be computed from extensive ray tracing from section II. Straighforward solution with Comsol Multiphysics indicate that the hot spot does not spread out. In section IV we discuss the remedy of changing the anode tapering angle.

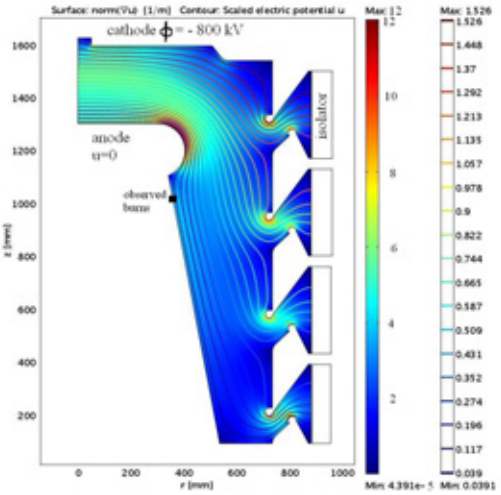

Figure 1: Simulation geometry, equipotentils

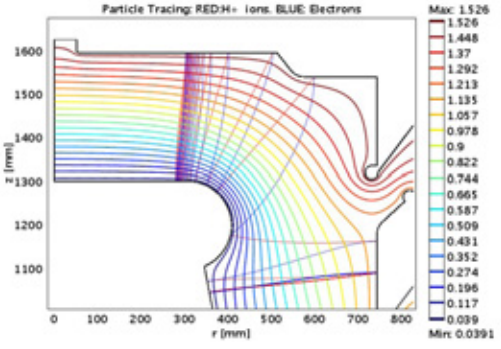

Figure 2: A cascade of H^+ and e for 40 iterations

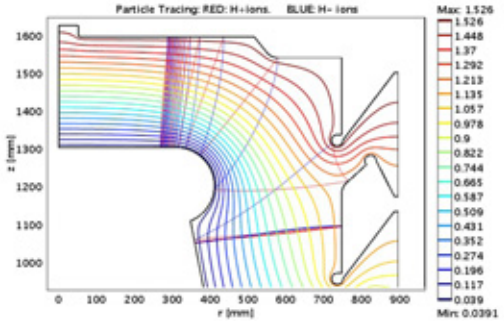

Figure 3: A cascade of H^+ and H^- for 40 iterations; starting position was tuned until two consecutive proton emission was observed; note anyway that acculumation point is as in fig 2

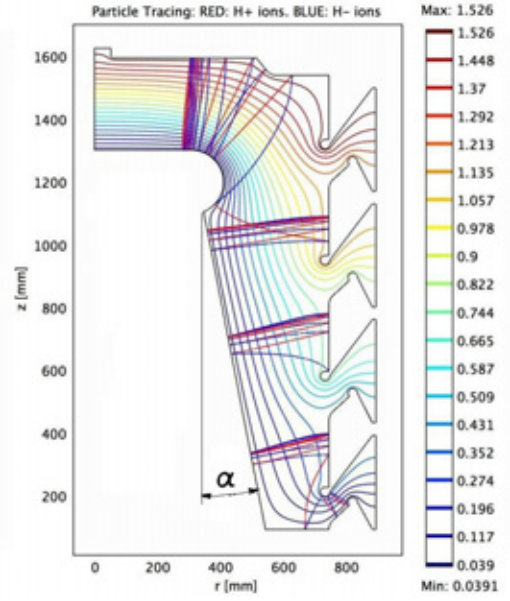

Figure 4: Three attrator; cascade consists of 35 iterations

2 The axisymmetric model

A realistic (even if not fully detailed) geometry was prepared and edited in the 2D dxf format (see fig 1); the system is axially symmetric around z and eventual misalignments were not studied. Let $r\theta z$ be a system of cylindrical coordinates. Isolators are made of fiberglass. Simulation of the electric potential ϕ is straighforward; note that potential energies and electron rest energies $m_e c^2$ are comparable, so that the scaled potential is here defined as $u = -e\phi/m_e c^2$.

Here a trajectory is the motion from one electrode to another, an orbit is a connected sequence of trajectories starting from the anode until the first time that it returns back to the anode or until it escapes from the system or it reaches an isolator. Since we have several cathodes (at different voltages), at any electrode the emitted particle charge sign is assumed equal to the sign of $u_{,n}$ where n is the inward normal (for later consistency). At isolators, tracking is stopped (since a more complicate physics will be added in future models). Mass of negative and positive particles is assigned by the user.

Fully relativistic equations of motions are given in Appendix, with m the particle mass, ie the particle charge and $s = ct(m_e/m)^{1/2}$ a convenient scaled time. Assuming now azimuthal symmetry of u and no magnetic field, we have that $L_1 = \gamma r^2 \theta_{,s}$ is constant on a trajectory, so that trajectory equations simplify to

$$\begin{aligned} r_{,ss} &= \frac{L_1^2}{\gamma^2 r^3} + \frac{i}{\gamma}\left[u_{,r} - \frac{m_e}{m} r_{,s} w\right] \\ z_{,ss} &= \frac{i}{\gamma}\left[u_{,z} - \frac{m_e}{m} z_{,s} w\right] \end{aligned} \qquad (1)$$

with $w = r_{,s}u_{,r} + z_{,s}u_{,z}$; note that $\gamma = \gamma_1 - i(u_1 - u)(m_e/m)$ with u_1 and γ_1 the initial values. Eq 1 is passed to '`postplot`'; for convenience and verification, we add

$$\theta_{,ss} = -[2(r_{,s}/r) + i(m_e w/m\gamma)]\theta_{,s}$$

2.1 Results of simple iterations

The simple iteration model consists in assuming that particles are emitted with zero speed, so at each impact (or iteration), one trajectory stops and another starts. This is convenient for plotting many iterations in the same figure, as shown in fig 2 and 3. Note that all particles rapidly acquire a velocity perpendicular to the electrode since this is the **E** direction; moreover in this case $L_1 = 0$ and θ is thus constant. In some cases, the orbit bounces between cathodes for some iterations before resuming the usual anode-cathode cycle of bouncing, as seen 3. Also many starting positions can be traced at the same time, so that the distance of two particles can be monitored.

This kind of simulations shows the existence of some accumulation points, corresponding to the attractors of the problem, where the orbit start point coincides with the orbit end point, so that the same orbit is always repeated. In the particular geometry

studied, different attractors can be found, in correspondence with the different intermediate electrodes, as shown in Fig 4; each one influences the motion of particle emitted in the neighboring positions. Moreover the upper intermediate electrode has a stronger attractor, since it has a higher energy and a better position, allowing it to collect cascades of trajectories originating from most of the upper region. Other simulations were performed setting the normal emitted velocity to a nonzero value, introducing the free parameters $\mathbf{K}$, that is the fraction of the parent particle speed which is transmitted to the emitted particle velocity. Variations in $\mathbf{K}$ only result in a little displacement of the attractor position, which seems to holds all its properties, up to values of $|\mathbf{K}| < 0.5$. Since values over this high limit seem to be unphysical, we can conclude that attractors always exists, in 2D analysis.

Effects of earth magnetic field and of electrode misalignmet should be included in future studies.

3 3D statistical average

As a second and more detailed analysis, we take into account the spread of re-emitted particle velocities and the consequent 3D motion.

At any point x_1 on the anode, we define a coordinate system for the emitted H^+ velocity $\mathbf{v}_1$; the components are v_n the velocity projection on the inwards normal (in the r, z plane) and $v_a = r\dot{\theta}$ the azimutal velocity and v_t, the component perpendicular to them. Note that v_t therefore stays in the r, z plane and is tangential to the electrode. The start point x_1 is here indicated by the surface coordinates b_1, θ_1 where b_1 is the arclength on the anode (from the axis). Of course the cylindrical components $r_1 = r(b_1)$ and $z_1 = z(b_1)$ are easily retrieved from geometry information.

Emission of particles in principle depends from the impact angle; since this is fairly near to the normal in most cases, we neglect this difference and thus have a distribution symmetric around the normal. It also depends on impact energy, which is piecewise constant (it depends on electrode voltage difference), so to simplify notation, we use emission distributions which are independent from x_1. Let $\mu_+ g_1 \mathrm{d}^3 v_1$ be the average number of H^+ emitted in a $\mathrm{d}^3 v_1$ inifitesimal element; in other words the integral of the distribution g is 1 by definition. Firstly we use a maxwellian model

$$g_1(\mathbf{v}_1) = k_1 \exp \frac{v_n^2 + v_t^2 + v_a^2}{2v_{s1}^2} \quad v_n \geq 0 \quad (2)$$

with k_1 a normalization constant and $v_{s1} = \sqrt{T_s/m}$ where T_s is the emission (or sputter) effective temperature; here $T_s = 25$ eV so $v_{s1} = 48.9$ km/s. Since g_1 is passed to CM as a string, user can easily modify this function. Similarly g_2 is the probability distribution of the initial velocities at the next impact (on the cathode).

Typically the third impact is on the anode again at a point $x = x_f(x_1, \mathbf{v}_1, \mathbf{v}_2)$ after a transit time $t_t(x_1, \mathbf{v}_1, \mathbf{v}_2)$, so that our orbit history is $h_2 = \mathbf{v}_1, \mathbf{v}_2$; in principle we can consider longer sequences h_n before returning to the anode. The probability of an element $\mathrm{d}w$ in the hystory space is the product of emission probabilities; for 2-impacts orbit this is $\mathrm{d}w(x_1, \mathbf{v}_1, \mathbf{v}_2) = g_1(v_1) g_2(v_2) \mathrm{d}^3 v_1 \mathrm{d}^3 v_2$

Let us define the most important statistical quantities. The probability of a displacement x_d on the anode is

$$W(x_1, x_d) = \int \mathrm{d}w(x_1, \mathbf{v}_1, \mathbf{v}_2) \delta(x_f - x_1 - x_d) \quad (3)$$

where x_f has same arguments of $\mathrm{d}w$. The loss probability is $B = 1 - A$ where

$$A(x_1) = \int \mathrm{d}x_d W(x_1, x_d) \quad (4)$$

The anode return frequency is

$$\nu(x_1) = \int \frac{dw(x_1, h_n)}{A(x_1) t_t(x_1, h_n)} \quad (5)$$

The displacement probability moments $M_{mn}(x)$ are

$$= \int \frac{\mathrm{d}w(x, \mathbf{v}_1, \mathbf{v}_2)}{A(x) t_t(x, \mathbf{v}_1, \mathbf{v}_2)} (x_d^1)^m (x_d^2)^n |_{x_d = x_f - x} \quad (6)$$

remembering that $x^1 \equiv b$ is the arclength on the anode and $x^2 \equiv \theta$ is the azimuth.

3.1 Fokker Planck approximation

The vector field (on the anode surface)

$$V(x) = (M_{10}(x), r M_{01}(x)) \quad (7)$$

with M_{ij} defined in eq. 6 has the meaning of the average velocity with which a spot of H^+ emission moves on the anode.

At a given time t, let $f(x_1, t)$ be the number (per unit anode area and multiplied by $A(x_1)$) of H^+ whose last anode emission was at x_1 plus the number of H^- (multiplied by $A(x_1)/\mu_2$) generated by an H^+ whose last anode emission was at x_1. This elaborate definition allows to write a master equation for f. For average displacements V/ν very much smaller than the average spread, the master equation can be simplified to a Fokker Planck equation. In the marginal stability regime, this equation becomes

$$\nu f = a_e + \mu A\{\nu f - \partial_x^i[V_i f - \partial_x^j(D_{ij} f)]\} \quad (8)$$

with sums implied on indexes i and $j = 1, 2$; here D is the diffusion tensor including the moments M_{20}, M_{11} and M_{20} and a_e represents any external inputs of H^+. Note that μ can be considered as an eigenvalue, which is the multiplication factor necessary to have a solution that neither grows nor decays with time. For a preliminary analysis, we extrapolate eq 8 even for large average displacements V/ν.

3.2 FP solution

Fokker Planck can be easily solved by a second application in Comsol Multiphysics[7], after coefficients $V_i(x)$ and $D_{ij}(x)$ are calculated by an extensive postprocessing of the solution in fig. 1, with steps here illustrated.

Fig 5 shows histories starting from two points, note the black square markers at the return points x_f. Fig 6 gives the W displacement probability with $b_1 = 0.4$ m. Note that W has a nice gaussian shape as expected; its computation was possible by sampling the 6D integrand of eq 3 in a lattice L of 717409 points, or histories; actually x_f values were computed for only 324 combinations of $\mathbf{v}_1$ and $\mathbf{v}_2$ by particle tracing and extended to the lattice L by interpolation.

At another point $b_1 = 0.37$ m (near the higher surface field region) there is a greater dispersion of x_f, so that W shape is no longer nicely gaussian, see Fig 7.

Fig 8 shows an overnight calculation, with trajectories from 150 points for b_1. Statistical moments are much faster to compute than W; fig. 9 showing only the first V component for graph readability is thus based

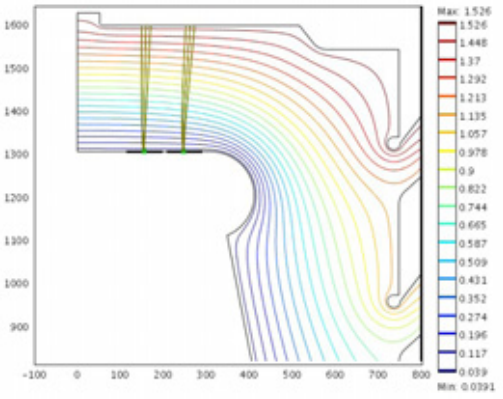

Figure 5: Two impact histories: note the H^+ paths (green) and the H^- return points on the anode (black squares); sputter temperature T_s greatly exaggerated for visiblity

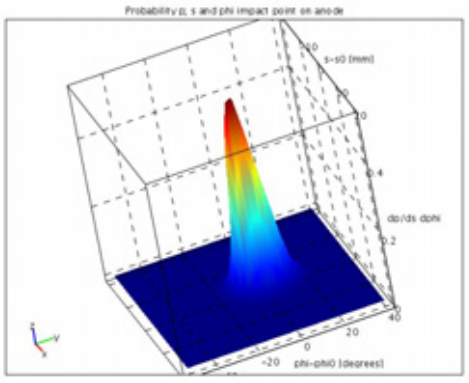

Figure 6: Displacement probability $W(x_1, x_d)$ vs x_d for $b_1 = 0.4$ m

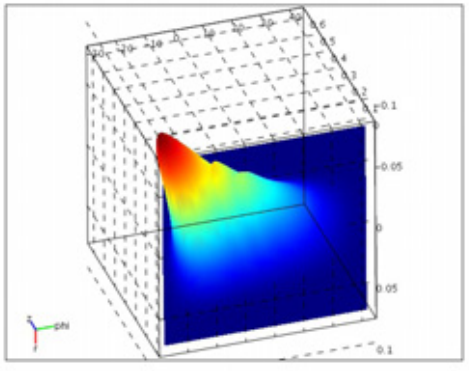

Figure 7: Displacement probability for $W(x_1, x_d)$ vs x_d for $b_1 = 0.37$ m

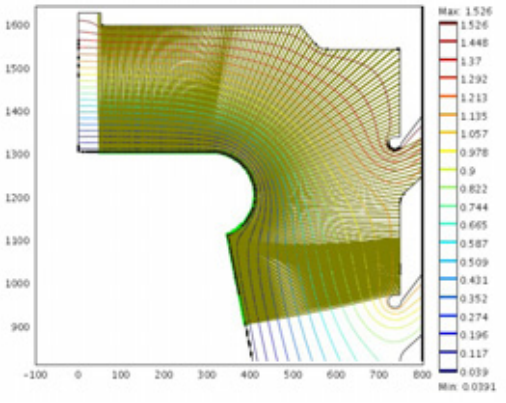

Figure 8: Accumulation of orbits

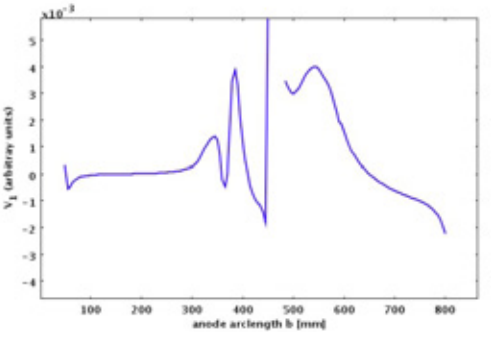

Figure 9: The velocity coefficient of eq. 8 for $\alpha = 191$ mrad; oscillations are near regions where some particle is lost

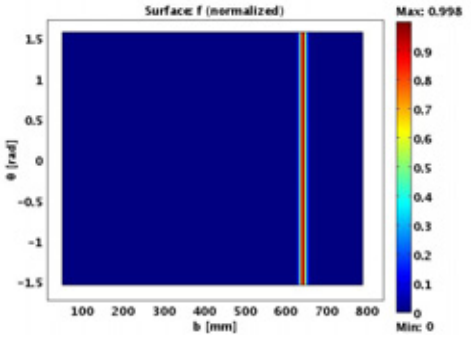

Figure 10: Eigenfunction for f with azimuthal number $m = 0$

on 107611350 integration points (150 choices for b_1, 847 for $\mathbf{v}_1$ and 847 for $\mathbf{v}_2$), each one equivalent in some sense to a Monte Carlo history.

Note that for azimuthal symmetry, results are independent from the starting value of θ_1; anyway, there is also a spreading in the azimuthal direction. The azimuthal symmetry implies that an eigenfunction corresponding to the lower μ value does not depend on θ; we label it by the wavenumber

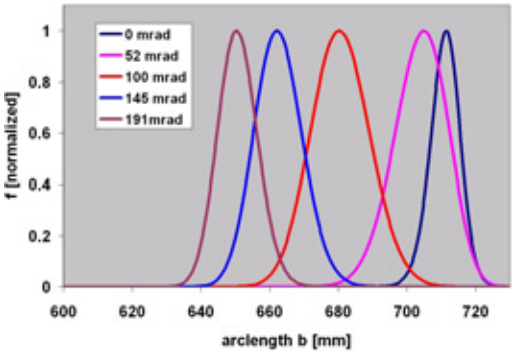

Figure 11: Eigenfunction profiles for $m = 0$ and tapering angles α listed in the legend (zoom near maximum).

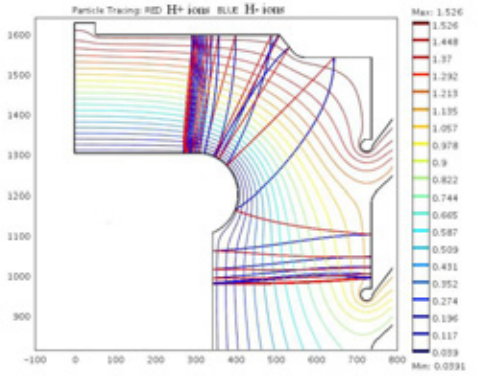

Figure 12: Attrator with tapering angle $\alpha = 0$

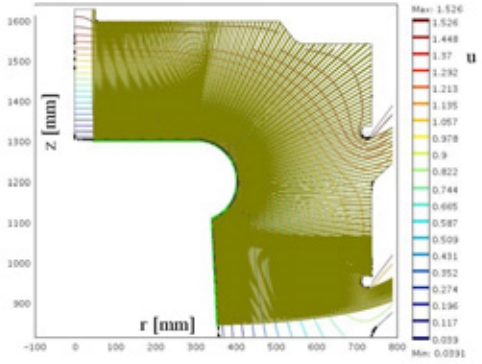

Figure 13: Accumulation of orbits with anode base radius $r_b = 400$ mm

$m = 0$; this eigenfunction of f shown in fig. 10 confirms that f peaks at a definite arclegth b_m on the anode, well corresponding to the attractor.

4 Geometry changes and conclusions

With the purpose of studying the effects of attractors on different geometries, further

analyses were performed. In particular the tapering angle α (the semi aperture of the conical support of the anode electrode, as defined in fig. 4) was changed assuming the values reported in table I; since we kept the top part of the anode unchanged, the radius of base of the conical support r_b changes with α. The main effect of such variation is again a displacement of the attractor position, which however maintains all its properties even in the $\alpha = 0$ case (cylindrical anode support). Moreover when $\alpha = 191$ mrad to make our geometry similar to the real NBI device mentioned in the introduction[6], the attractors position fits well the melting points found experimentally. This confirms the capability of cascade attractors to predict the electrodes damages caused by microdischarges.

Note that for each α the anode coordinate b_m of the f eigenvalue maximum found by the statistical approach always agrees the accumulation point b_a of the 2D simple iterations. The 3D nature of this statistical approach will allow to better include further effects in the pingpong model, like perturbations of external magnetic field, misalignement and overheating.

α [mrad]	r_b [mm]	b_m [mm]	b_a [mm]
0	347	711.44	716.20
52	400	704.93	705.57
100	449	680.40	677.47
145	494	662.27	659.09
191	543	650.39	649.94

Table 1: Variation of the attractor position b_m and b_a as function of the tapering angle α or the anode base radius r_b

References

[1] W. K. Mansfield, British Journal Of Applied Physics 11 454 1960

[2] H.R. Mc K. Hyder Rev. Phys. Appl. (Paris) **12**, 1493-1501 (1977)

[3] L. Cranberg, Jour. Apl. Phys., **23**, 538 (1952)

[4] B P Singh, P A Chatterton, "A new model of microdischarge current growth in vacuum", *J. Phys. D*, **9**, 1797 (1976)

[5] T. Inoue et al., "1MeV, ampere class accelerator R&D for ITER", Nucl. Fusion 46 (2006) S379

[6] M.Taniguchi et al., "SINGAP test at JAEA MeV test facility", in JA-EU workshop Dec.12-15, 2007, JAEA NAKA

[7] W. B. Zimmerman, *Multiphysics modelling with finite element methods*, Singapore, World Scientific, (2006).

[8] G. Fubiani, H. P. L. de Esch, A. Simonin, R. Hemsworth, Phys. Rev. ST-AB, **11**, 014202 (2008)

Appendix

The relativistic equation of motion $\mathbf{F} = m\mathrm{d}_t(\gamma\mathbf{v})$ with m the particle rest mass becomes (by expanding the derivatives)

$$\mathbf{F}/m = \gamma[\mathbf{a} + \gamma^2\beta(\beta\cdot\mathbf{a})] \tag{9}$$

or solving eq 9 for the acceleration $\mathbf{a}$

$$\mathbf{a} = \gamma^{-1}[(\mathbf{F}/m) - \beta(\beta\cdot\mathbf{F}/m)] \tag{10}$$

Now the acceleration is

$$\mathbf{a} = \hat{r}(\ddot{r} - r\dot{\theta}^2) + \hat{\theta}(r\ddot{\theta} + 2\dot{r}\dot{\theta}) + \hat{z}\ddot{z} \tag{11}$$

in cylindrical coordinates. With no magnetic field

$$\mathbf{F}/m = ie\mathbf{E}/m = i(m_e/m)c^2\nabla u \tag{12}$$

Substituing eqs. 11 and 12 into eq. 10 and using s definition, we get

$$\hat{r}(r_{,ss} - r\theta_{,s}^2) + \hat{\theta}(r\theta_{,ss} + 2r_{,s}\theta_{,s}) + \hat{z}r_{,ss} = i[\nabla u - (m_e/m)\mathbf{x}_{,s}w]/\gamma \tag{13}$$

with the shorthand $w = r_{,s}u_{,r} + z_{,s}u_{,z} + (\theta_{,s}u_{,\theta}/r^2)$; this form is numerically convenient both for electrons and protons.